

ANTECEDENT EVENTS UNDERLYING AXON DAMAGE IN AN ANIMAL
MODEL OF MULTIPLE SCLEROSIS

A RESEARCH PAPER

SUBMITTED TO THE GRADUATE SCHOOL

IN PARTIAL FULFILLMENT OF THE REQUIREMENTS

FOR THE DEGREE

MASTERS OF SCIENCE

BY

MARY BRINKOETTER

DR. DERRON BISHOP – ADVISOR

BALL STATE UNIVERSITY

MUNCIE, INDIANA

JULY 2009

Acknowledgements

Thank you to my committee. I thank Dr. Derron Bishop for being an outstanding thesis advisor. His dedication to his research, his passion for science, and his candid real world advice have been invaluable to me. Because of him, I look forward to my future and can only hope that I find as much joy and purpose in my career as he finds in his teaching and research.

I thank Dr. Susan McDowell for being not only a wonderful and dedicated teacher, but also a caring mentor. Over the past two years, she has given me her time both in and out of the classroom. I truly appreciate her dedication to the well being of her students.

Thanks to Dr. Heather Bruns for being a great teacher and for being such a positive person. Her light hearted style of teaching makes learning fun and appealing.

I thank Sharmon Knecht for her support in my research project and in life. She has been a fantastic friend, editor, and colleague. It has been a pleasure working side by side with her, and I look forward to many years of our friendship to come.

Thanks to Dr. Martin Kerschensteiner, Dr. Thomas Misgeld, and Ivana Nikić for allowing me to be a part of such an interesting project.

Thanks to Dr. David LeBlanc for his statistical analysis expertise.

I thank Joshua Schum for his technical support and for his emotional support during a very tough year. Finally, thanks to my loving family without whose unconditional encouragement I would be lost.

Table of Contents

	Page
Introduction	1
Myelin and Demyelinating Diseases	1
Cellular Mechanisms of Multiple Sclerosis and Demyelination	3
Animal Models of MS	6
Materials and Methods	11
Animals	11
Near- Infrared Burning	12
Fiducial Markers	13
Electron Microscopy	14
Reconstruction	15
Axon Ultrastructure Evaluation	16
Myelin Removal	17
Controls	17
Results	19
Correlative Light and Electron Microscopy- Near-Infrared Burning (NIRB)	19
Axon Ultrastructure Evaluation	21
Mitochondrial Shape Factor	23
Disruption of Cytoskeletal Arrangement	25
Discussion	29
Near-Infrared Burning (NIRB)- A novel approach to correlative Light and electron microscopy	30
Mitochondrial Pathology underlies a unique mechanism of axon Degeneration	32
Cellular Mechanisms of Demyelination	33
References	36

List of Tables

1. Axons from experimental autoimmune encephalomyelitis (EAE) axons contained a higher proportion of damaged mitochondria than control axons. Page 38.
2. Mitochondria from control axons contained a smaller proportion of damaged mitochondria than experimental autoimmune encephalomyelitis (EAE) axons. Page 39.
3. Mitochondrial shape factor was significantly lower for normal mitochondria within each group (EAE and control); shape factor for normal and damaged mitochondria was lower for EAE axons as compared to their control axon counterpart groups. Page 40

List of Figures

1. Figure 1. Laser-induced Fiducial Markers. Page 41.
2. Figure 2. Correlated light and electron microscopy show early mitochondrial morphological changes in experimental autoimmune encephalomyelitis (EAE) axons. Page 42.
3. Figure 3. Correlated light and electron microscopy show early mitochondrial morphological changes in experimental autoimmune encephalomyelitis (EAE) axons. Page 43
4. Figure 4. Correlated light and electron microscopy show normal mitochondrial morphology in a representative axon from control animals. Page 44.
5. Figure 5. Shape factor of normal and damaged mitochondria is lower in EAE axons as compared to their control axon counterpart groups. Page 45.
6. Figure 6. Disrupted cytoskeleton in EAE axons. Page 46.
7. Figure 7. Demyelination through delamination of multiple myelin layers. Page 47.

Introduction

Efficient communication between neurons is predicated upon the ability to conduct high velocity electrical signals down the axons. Such high velocity signaling is essential for quickly creating motor outputs in response to external stimuli (such as withdrawing your hand from a hot object) or processing vision in near real time. Without high conduction velocity, not only is reaction time diminished, but the intricate timing and processing of electrical signals in the brain becomes compromised. In simple nervous systems, such as in insects, the problem of conduction velocity is solved by building large diameter axons. This strategy works well in relatively small animals that have few neurons. In the more complex vertebrate nervous systems that contain an additional $\sim 10^8$ neurons, this strategy is untenable necessitating an exceedingly large skull to contain the brain. This problem is solved through axons interaction with support cells known as glial cells. Smaller diameter axons are wrapped with nonconductive glial cell membrane in concentric layers known as myelin. Although myelin serves to increase conduction velocity in a small diameter axon, it is also susceptible to pathological processes that have profound consequences to the functioning of the nervous system.

Myelin and Demyelinating Diseases

Myelin is a multilayer lipid membrane wrapped around the axon (referred to as myelin sheath) by oligodendrocytes in the central nervous system (CNS)

and Schwann cells in the peripheral nervous system (PNS) (D. L. Sherman and P. J. Brophy, 2005). The myelin sheath facilitates rapid action potential conduction by decreasing capacitance between the intracellular and extracellular membrane of the axon (separating opposite charges of each environment). Myelin is not continuous along the entire length of the axon. The nodes of Ranvier are unmyelinated patches of axon membrane where ion channels regulate the ionic flux across the membrane. Action potentials are generated at these nodes when a specific threshold of depolarization is reached. The charge propagates axially along the inner membrane surface of the axon. Without the myelin sheath, the action potential of the axon is slowed or blocked entirely because the capacitance between the intracellular and extracellular environment is increased, and the charge of the action potential is likely to leave the cell as capacitive current instead of continuing down the axon.

Although the vertebrate strategy of myelination solves several evolutionary problems, there are a few drawbacks. In particular, there are a number of pathological situations where myelin can become stripped from the axon reducing conduction velocity or even causing a complete conduction block. Perhaps the most common of these so-called demyelinating diseases is multiple sclerosis (MS), named for the sclerotic appearance of postmortem nervous system tissue in patients with the disease. MS primarily manifests in the CNS and is characterized initially by impaired neurologic function (R. Dutta and B. D. Trapp, 2007) such as limb weakness, loss of vision, double vision, and

ambulatory instability (S. L. Hauser and J. R. Oksenberg, 2006). As the disease progresses, severity of symptoms increases and patients may experience bladder dysfunction, facial weakness, vertigo, and even cognitive deficits.

The progression of MS is not monotonic. That is, in the early phase of the disease a patient generally presents with a relapsing-remitting (RRMS) phase that oscillates between periods of neurologic decline followed by periods of recovery. Although the RRMS phase can persist for many years, it eventually gives way to a secondary-progressive (SPMS) phase (C. Bjartmar et al., 2003) characterized by irreversible neurologic decline.

Cellular Mechanisms of Multiple Sclerosis and Demyelination

The cellular and molecular mechanisms responsible for conferring disease onset and progression have not been fully elucidated. One of the main difficulties is related to the notion that the RRMS and SPMS phases may have different cellular and molecular underpinnings (B. D. Trapp et al., 1999; C. Bjartmar et al., 2003), or may be a single etiologic disease with a biphasic symptoms (R. Dutta and B. D. Trapp, 2007). Although immune-mediated demyelination is the hallmark of the MS, it is likely not the major cause of clinical symptoms in both phases of the disease since anti-inflammatory or immunomodulatory agents that benefit those in the RRMS phase provide little therapeutic value to patients with SPMS phase of the disease (D. Papadopoulos et al., 2006). From this observation, it is thought that axon loss is the primary

cause of symptoms. Further, some demyelinated axons recover and even remyelinate (B. Kornek et al., 2000; C. Bjartmar and B. D. Trapp, 2001; C. Bjartmar et al., 2003), whereas other axons can become damaged independent of demyelination (D. Papadopoulos et al., 2006). It is not until axons are irreversibly damaged during the SPMS phase that neurologic function progressively declines with no periods of recovery. The important missing information in understanding the conversion from the RRMS to SPMS phase is the relationship (causal and chronological) between demyelination, direct immune cell interaction and axon loss (T. Misgeld and M. Kerschensteiner, 2006).

Because axons contain no protein synthetic organelles, the bulk of axonal contents are mitochondria and cytoskeleton (A. B. Knott et al., 2008). Mitochondrial and cytoskeletal dynamics, therefore, become important mediators of neuronal and axonal homeostasis and potential disease mediators. Recent evidence supports the idea that mitochondrial bioenergetics largely dictate an axon's fate (X. Qi et al., 2006). Mitochondria are known to release proapoptotic factors (K. Thress et al., 1999), and the organelles are also the major source of reactive oxygen species (ROS) in an axon (B. Kalman et al., 2007). It is possible that during progression of the disease, localized breakdown of mitochondria could signal the release of proapoptotic factors such as cytochrome C (A. B. Knott et al., 2008) and/or the release of ROS creating a toxic internal environment causing the axon to take the path of inevitable death. Classically, these pathways have been described in developmental neuronal cell death, but

have more recently been implicated in several neurodegenerative diseases including Huntington's Disease (X. Wang et al., 2008) Alzheimer's Disease (C. Culmsee and S. Landshamer, 2006), and Parkinson's Disease (M. Vila and C. Perier, 2008; H. Bueler, 2009).

The cytoskeleton, as in other cells, is typically associated with transport. Axon transport, though, is particularly critical in axons considering they can be nearly one meter in length without the ability to synthesize proteins. Therefore, any small injury to a CNS axon is detrimental because any protein needed to repair the injury would have to travel from the cell body to the injury site which could take several days depending on the length of the axon. Amyotrophic lateral sclerosis (ALS) is one such disease where transport deficits due to disrupted neurofilaments are thought to mediate the disease (T. L. Williamson and D. W. Cleveland, 1999). In the case of ALS, target derived neurotrophic factors necessary for survival cannot be transported retrogradely from axon terminals to the nucleus. Such disruption in the trophic support often leads to activation of cell death pathways (R. R. de la Cruz et al., 1996).

Although little is known about axon loss in MS, it is possible that these cellular mechanisms may similarly be involved. In particular, there is evidence for mitochondrial changes during demyelination. Myelin thinning/loss can initially inhibit an axon's ability to generate action potentials. To compensate, channels that are normally restricted to the node migrate to span the length of the axon (S. L. Hauser and J. R. Oksenberg, 2006). The energy requirement of the cell increases during this time and mitochondria, which supply energy for the ion

channels and the cell's general activity, tend to accumulate at these sites of demyelination (S. E. Mutsaers and W. M. Carroll, 1998). Although this highly localized concentration of mitochondria helps provide additional energy to maintain ionic balance across the cell membrane during demyelination, it is also possible they could serve as a target for mediating axon destruction.

Animal Models of MS

In order fully understand all aspects of the progression of axon loss during MS, it would be ideal to view a degenerating axon over time in a living system. Such unprecedented access would permit the temporal characterization of events that underlie axon degeneration. For instance, whole axons could degenerate as in the case of Wallerian degeneration (B. Beirowski et al., 2005) or axonal contents could be dispersed within individual fragments as is the case in axosome shedding (D. L. Bishop et al., 2004). It is also possible that localized apoptotic driven degeneration is responsible for EAE axon degeneration. Each of these mechanisms is classified by distinct cellular and subcellular conditions. The former is represented by loss of cytoplasmic density along with disrupted mitochondria and cytoskeleton. The latter typically shows a much less destructive milieu with large spherules of axon become engulfed by nearby glia. If none of these known mechanisms of degeneration is obvious, it is possible that EAE axon degeneration is a novel process. Understanding the mechanism of degeneration could lead to a possible therapeutic target. Unfortunately, these

types of studies are not possible in humans due to both technical and ethical restraints. Most analysis of tissues in human MS patients relies upon either postmortem tissue that lacks structural preservation, or non-invasive imaging procedures (PET scanning, MRI, etc.) that lack resolution.

It is with these ideas in mind that the experimental autoimmune encephalomyelitis (EAE) mouse model was created (T. M. Rivers, 1935). While this animal model does not mimic human MS entirely, it serves as a tool to research certain aspects of MS (D. S. Skundric, 2005). The EAE mouse model is created by immunization against CNS myelin proteins. Specifically, EAE mice are immunized with a recombinant form of myelin-oligodendrocyte glycoprotein (rMOG) (M. Kerschensteiner et al., 2004). The result is an immune reaction against CNS myelin resulting in multifocal demyelination and axon damage (D. S. Skundric, 2005). The EAE mouse model presents the same RRMS symptoms as human clinical RRMS, and has been effective in developing current therapies for MS (S. L. Hauser and J. R. Oksenberg, 2006).

While these mice permit both cellular and molecular analysis during the onset and progression of MS, a particularly powerful approach recently has been combining these animals with additional lines of transgenic mice. In particular, transgenic mice expressing variants of green fluorescent protein (GFP) in the cytoplasm of their neurons (G. Feng et al., 2000) can be immunized against rMOG to create mice with fluorescent axons that are susceptible to immune mediated demyelination and axon loss. Using time-lapse multiphoton, *in vivo*

imaging following a laminectomy to expose the spinal cord (T. Misgeld et al., 2007), it is possible to watch individual axons over time during the onset and progression of axon loss associated with EAE. Drs. Martin Kerschensteiner and Thomas Misgeld have pioneered such an approach (T. Misgeld and M. Kerschensteiner, 2006; T. Misgeld et al., 2007) and observed axons through the course of their individual pathology. Their results indicate that the earliest stages of axon fragmentation are identifiable by focal axonal swelling in the paranode region (unpublished observations). This result suggests that the mechanism for degeneration is mediated focally at the paranode region.

There are numerous candidates that could mediate toxic properties focally at the paranode. In addition to mitochondrial and cytoskeletal abnormalities within the axon, it is also possible that the immune cells impose a detrimental interaction at the paranode. Distinguishing amongst the myriad of possibilities for how an axon can degenerate requires a methodological choice. One approach is to assay for all the specific cellular responses amongst the *in vivo* tissue with a battery of antibody markers using either microscopy or protein detection methods (i.e., Western blotting). This approach is problematic due to the sheer number of choices for the antibody (mitochondrial proteins, caspases, neurofilament subunits, etc.). This problem is further compounded by both the volume of tissue analyzed and the fact that both neuronal and non-neuronal tissue respond to the antibody. Assaying for cell death markers or other cellular processes is

problematic due to the notion that the sample comes from a non-homogenous population of cells that can be in various stages of the disease.

The alternative is to use electron microscopy to resolve the subcellular condition of a specific axon. This approach removes organelle and tissue specificity, but also creates a sampling problem. Traditional transmission electron microscopy (TEM) relies upon slicing extremely thin sections through small areas of tissue. The odds of slicing through tissue immediately prior to axon loss are exceedingly low in non-homogenous tissue. Randomized sectioning in diseased tissue, therefore, results in ambiguity in interpretation since any observation cannot be interpreted with knowledge of the axon state.

One way to solve these problems is to utilize serial section transmission electron microscopy (ssTEM) correlated to specific previously imaged spinal axons. Such an approach removes the sampling problem while also permitting ultrastructural observations to be interpreted without ambiguity. *In vivo* imaging is useful for viewing specific chronology and general morphology of events and structures in living models, but the resolution that TEM provides allows careful examination of subcellular organelles, internal structural components, and intercellular interactions of the diseased axon that light microscopy cannot.

Therefore, the primary focus of this project is to first develop a technique to correlate ssTEM reconstructions of specific axons to *in vivo* microscopy thereby permitting highly resolved electron micrographs to be placed in both a temporal and macroscopic context. The second focus will be to use this

technique to target axons in EAE animal model of MS prior to axon degeneration
in an attempt to uncover cellular processes that underpin axon loss.

Materials and Methods

Animals

Drs. Misgeld (Technical Institute for Neuroscience- Munich) and Kerschensteiner (Ludwig-Maximilians-University, München, Germany) have provided fixed vibratome sections of vitally imaged spinal cords (*T. Misgeld et al., 2007*). All surgical and imaging procedures were approved by the local Institutional Animal Care and Use Committee (protocols 209.1-211-2531-101-05/ 127-05/ 93-06/ 94-06/ 74-07/ 81-07/ 25-08 filed with the Government of Upper Bavaria - Germany/ Regierung von Oberbayern). Double transgenic *thy1* green fluorescent protein (GFP) S-line X *thy1* Mito cyan fluorescent protein (CFP) S-line mice were immunized with rMOG. *Thy1*- GFP-S line mice exhibit cytoplasmic expression of subsets of neurons in the dorsal column to allow identification of single neurons. *Thy1*-CFP-S line mice exhibit expression of neuronal mitochondria. For two photon *in vivo* imaging, mice were anesthetized and placed on a heated cushion for surgery. Mice were intubated to maintain respiration once a plane of anesthesia was established. A dorsal midline incision was made to expose the dorsal surface of the spinal cord. Individual axons in the dorsal column became visible following a laminectomy. After surgery, animals were transferred to the imaging stage of a two-photon/wide-field epifluorescent microscope. Images were captured of single axons at 15 minute intervals for up to 6 hours on as many as 5 consecutive days.

After *in vivo* imaging, mice were sacrificed and perfused transcardially with Tyrode's solution to exsanguinate followed by 2.0% paraformaldehyde + 2.5% glutaraldehyde in 0.1% sodium cacodylate buffer. The spinal cord with axon of interest was carefully dissected and embedded in agar. Longitudinal vibratome sections of the spinal cord were sliced (~150 μ m) and mounted on a glass microscope slide with sodium cacodylate buffer under a sealed coverslip.

Near-Infrared Burning (NIRB)

A Ti: sapphire mode locked laser was used to create fiducial markers around the region of interest. The wattage of the laser (1.6 Watts) was adjusted so that an 830 nm beam could generate enough heat to burn the tissue. The laser beam could be scanned to create a burned box around the region of interest. In addition, a marker point was burned for recognition at both the light and electron microscopic level (see electron microscopy section). The burned edges of the box exhibited red autofluorescence that could be made electron dense (see below). The advantage of using this technique is the markers can be adjusted in the X, Y, and Z dimension. Two experimental mice (one axon each) and one control mouse (4 axons) were imaged and provided for ssTEM.

Fiducial Markers

In addition to the laser burned NIRB markers, an additional marker was added to the tissue. Vibratomed spinal cord sections were removed from the slides and placed in 35mm Petri dishes (Corning Glass Works, Corning, NY) lined with Sylgard silicone elastomer (Dow Corning Corporation, Midland, MI). The spinal cord sections were pinned with fine minutien pins (Fine Science Tools, Foster City, CA) in sylgard-lined petri dishes for stabilization during iontophoresis and photoconversion.

Crystals of 1, 1'-dioctadecyl-3,3,3',3'-tetramethylindodicarbocyanine-5,5'-disulfonic acid (Dil, Invitrogen, Carlsbad, CA) were applied to the surface of the spinal cord slice next to the axon of interest. A 1.0% solution of Dil in 100% dicholormethylene (Sigma-Aldrich, St. Louis, MO) was loaded into a micropipette (World Precision Instruments, Sarasota, FL) pulled to a resistance of 5-10 M Ω with a micropipette puller (Kopf, Tujunga, California). The pipette was threaded with a silver chloride electrode attached to a SD9 stimulator (Grass Instruments, Quincy, MA). The microelectrode was used to impale the spinal cord axons near the NIRB fiducial marker and electrical pulses (5V at 10Hz) were passed to the ground (bath) electrode. These electrical pulses caused a crystal of Dil to form at the microelectrode tip and within the tissue of interest.

To render both the Dil crystal and laser-burned fiducial markers electron dense, 3, 3' -Diaminobenzidine (DAB, 5.0mg/mL, Sigma-Aldrich) was used to photoconvert the crystal. DAB was dissolved in cold, ultrapure water and added

to the plate containing the spinal cord slices. Areas of interest were re-located on an Axioskop fluorescent microscope (Zeiss, Maple Grove, MN) and photo-oxidized by exciting the Dil crystal near its excitation wavelength for ~20min with an achroplan 40x, 0.80W water immersion lens (Zeiss). The Dil crystal and autofluorescent laser-burned NIRB markers were replaced with a dark red/brown DAB precipitate.

Electron Microscopy

After photoconversion, spinal cord slices were trimmed to contain the axon of interest and electron dense fiducial markers (photoconverted Dil crystal and NIRB markers). Tissue blocks were stained with 2.0% osmium tetroxide (Electron Microscopy Sciences, Hatfield, PA) reduced in 3% potassium ferrocyanide (Sigma-Aldrich). Tissue blocks were washed with 4 changes of 0.1 M sodium cacodylate buffer (Electron Microscopy Sciences) and dehydrated in an ascending ethanol series (AAPER Alcohol and Chemical Company, Shelbyville, KY). After dehydration, tissue blocks were placed in 2 changes of 100% propylene oxide (Electron Microscopy Sciences). Tissue blocks were infiltrated with Araldite 502/ EMBED812 resin and polymerized at 60°C for 48 hours (Electron Microscopy Sciences).

Polymerized tissue blocks were trimmed into a trapezoid shape and thick sectioned (0.5µm) with a glass knife on a Leica Ultracut R microtome (Leica, Wetzlar, Germany). Thick sections were examined individually with an Axiovert

35M light microscope (Zeiss) to locate the fiducial markers. When a fiducial marker was located, the block was trimmed down to a smaller trapezoid to contain only the area of interest using a cryotrimming tool (Diatome, Hatfield, PA). The tissue was thin sectioned (60-70nm) into hundreds of serial sections containing the axon of interest with a diamond knife (Diatome) and a Leica EM UC6 ultramicrotome (Leica). Thin sections were placed on pioloform-coated (1.2% pioloform, Ted Pella, Inc. Redding, CA, in chloroform, Sigma-Aldrich) slot grids (Electron Microscopy Sciences).

Pioloform-coated grids (each with 1-6 thin sections on it) were counterstained with 2.0% aqueous uranyl acetate (Electron Microscopy Sciences) and Reynold's lead citrate. Sections were viewed at 75kV on a Hitachi H-600 transmission electron microscope. Serial images of the axon of interest were captured at 5000X on KODAK electron microscope film.

Reconstruction

Negatives were scanned with an Epson Perfection V700 PHOTO Scanner (Epson). Multiple images were montaged using PanaVue Image Assembler (PanaVue Inc., Quebec, Canada). Montaged photos of each section along with a calibration grid (for accurate measurements) were imported into Reconstruct (<http://synapse-web.org>). Section thickness is estimated using the cylindrical diameters method (J. C. Fiala and K. M. Harris, 2001). Sections were aligned,

and surface contours of items of interest (axons, mitochondria, etc.) were manually traced. These contours were tessellated into three dimensional wireframe VRML models and rendered using 3ds Max (Autodesk, San Rafael, CA). Individual sections were correlated with the 3D image and quantitative data were collected and evaluated (see below).

Axon Ultrastructure Evaluation

Mitochondrial ultrastructure was evaluated based on three criteria: 1. Are the cristae and mitochondrial membranes intact? 2. Do the mitochondria have normal cytoplasmic electron density? 3. Are there any swollen cristae or vesiculation? Mitochondria were considered normal if cristae are intact, electron density is normal, and no swelling occurs or if only one or two of these three characteristics is compromised. Mitochondria were considered damaged if all three characters are compromised. Proportions of damaged mitochondria between EAE and control axons were analyzed by Fisher's exact test.

Mitochondrial shape factor, the ratio of length to width, was used as a second means of evaluation. Mitochondrion length and width were determined by measuring the section where a mitochondrion reached its maximum length or width respectively. Mitochondria that were cut in cross section were analyzed through multiple sections to facilitate these measurements. Mean shape factor for normal and damaged mitochondria in both EAE and control axons were

calculated. A two-tailed Student's t-test was used to analyze shape factor data for statistical significance.

The cytoskeleton was analyzed by focusing on the arrangement of neurofilaments. Neurofilaments are normally arranged axially in the axon and with our longitudinal sections should appear parallel to each other. Areas where they become disorganized were identified and compared between EAE and control axons.

Myelin Removal

Macrophage mediated demyelination was analyzed by focusing not only on the axons imaged *in vivo* and targeted for ssTEM reconstruction, but also nearby axons that have clear macrophage interactions. Axons were analyzed from both EAE animals and the control animal. The macrophage/myelin interface was identified by locating areas where macrophage and axonal membranes were in direct apposition. Active internalization of myelin or myelin removal was identified by analyzing myelin integrity (delamination, abnormal configuration, complete detachment, etc.) and thickness (number of layers present at macrophage interaction site). Total observations of active myelin internalization were recorded and subsequently qualitatively analyzed.

Controls

Because of the heterogeneous effect of the disease and subsequently the EAE mouse model (not all axons undergo the same course of pathology), it is necessary to implement the proper controls. Non-EAE animals from the same *Thy-1* GFP S-line were used as controls. This will primarily control for phototoxicity during *in vivo* imaging. Axons within the same control mouse but not labeled with GFP serve as a control to eliminate the possibility of axon damage due to fluorescent labeling or fixation artifacts.

Results

Correlative Light and Electron Microscopy - Near-Infrared Burning (NIRB)

Since the advent of multi-photon microscopy, numerous areas of biology have benefited from *in vivo* imaging that allows following complex cellular behaviors in the natural tissue habitat. One limitation, however, remains the moderate resolution of this technique (app. 0.5 μm in the x-y-dimension and worse in z), compared to the size of the subcellular machinery responsible for executing cellular behavior. Currently, electron microscopy (EM) remains the only technique that allows visualization of subcellular structures within the context of preserved tissue. Correlating electron microscopic analysis with *in vivo* microscopy, however, remains a major challenge, especially in complex tissues, such as the nervous system. This is due to the fact that correlated ultrastructural examination of a cell previously imaged *in vivo* requires the re-identification of this specific cell in the context of thousands of other similar, but irrelevant cells.

To overcome this technical difficulty, we developed a technique we call “*near-infrared burning*” (NIRB) that takes advantage of a multi-photon microscope’s ability to focus high intensity illumination in defined three-dimensional positions. The basis of the technique is the fact that highly focused, femtosecond-pulsed near-infrared light, as typically used for multi-photon excitation, can at higher intensities destroy fixed tissue and generate a burn mark that follows the laser-scan pattern. Using the scan mirrors of a commercial confocal scanner, points or lines at arbitrary positions or angles can be

introduced. The size of such burn marks can be controlled by limiting the dose of pulsed light exposure.

We introduced fiducial markers in vibratome sections of spinal cord following imaging and fixation of single fluorescently labelled axons from living transgenic mice (Figure 1). Vibratomed spinal cord slices were mounted on slides to provide a reproducible orientation to the *in vivo* view. By then sequentially selecting line scans of a femto-second pulsed titanium-sapphire laser (1.6W at 830nm) a few microns above, below, left and right of the axon of interest, we burned a square that surrounded the axon (Figure1C). We made sure that in the Z-dimension the burn marks were placed slightly (1-2 microns) above the axon of interest, to ensure that once the marks appear during trimming of the plastic-block for EM, the plane of section is still well above the first section of the target volume. A final mark (using a point scan) was set directly adjacent to the structure of interest but away from the area chosen for later electron microscopic reconstruction to provide a confirmation for successful re-identification.

Returning the slide to the confocal microscope, we again scanned the axon of interest. The resulting image stack, projected in X, Y and Z dimensions therefore served as a map for tissue sectioning by providing a rough distance from the tissue surface to the object of interest. We unexpectedly found that two-photon fiducial marks are autofluorescent with a characteristic spectral signature. We felt it might be possible for this autofluorescence to drive the photo-oxidation

of diaminobenzidine (DAB) to serve as an electron dense fiducial marker in the electron microscope. After illuminating the tissue in DAB-solution with 530-560nm band pass illumination we found the autofluorescence was completely replaced by an electron dense precipitate (Figure 1D).

The tissue was then processed for tissue embedding using standard protocols (See Methods). The blocks were trimmed and thin sections were cut using a glass knife until the photoconverted burn marks became visible. Ribbons of ultrathin sections were cut and collected and screened in the TEM until burn marks could be seen as sharp tissue defects surrounded by electron-dense precipitate. Images were then collected from serial sections and the target structure was identified by registering EM sections with the confocal or multiphoton documentation. Careful inspection of the resulting image stacks generally provided “candidate” structures, which could be confirmed or refuted based on tracing them to the expected site of the confirmatory mark placed next to the structure of interest. Using this iterative approach, we were successfully able to re-identify all of the myelinated axons we attempted in this study.

Axonal Ultrastructure Evaluation

Using this NIRB technique, we examined identified axons from EAE and control animals. The EAE axons exhibited signs of axon damage at the light microscopic level including focal swelling in the paranodal region and a small

outpocketing of GFP cytoplasm (Figure 2A, see arrow) compared to controls. Serial electron micrographs through EAE axons from two animals and four control axons from one animal were imported into Reconstruct for ultrastructural analysis.

We analyzed mitochondrial morphology in the paranode region of the target axons through multiple sections and categorized them based on three structural characteristics: cristae and mitochondrial membrane integrity, electron density, and vesiculation. Mitochondria were considered normal if 0-2 of these characters were compromised. Mitochondria were considered damaged if all three characters were compromised. Using these criteria, we classified mitochondria from two EAE axons, and found that in one axon 76 of 102 (56.2%) were damaged (Figure 2), and 18 of 32 (29.0%) mitochondria were damaged (Figure 3) in the other axon. Quantitative data for these two axons are summarized in Table 1.

Control axons from non-EAE mice were also analyzed to determine proportion of damaged mitochondria per axon (Figure 4). We examined both GFP and non-GFP axons as controls. Three control axons expressed GFP (Control axons 1, 2, and 3) and one control axon did not express GFP (Control axon 4). Control axon 1 had 3 of 33 (9.1%) damaged mitochondria in the reconstructed segment. Control axon 2 had 13 of 60 mitochondria damaged (21.7%). Control axon 3, did not have a single one of its 61 mitochondria damaged. Control axon 4, the only axon that did not express GFP, had only 2 of

its 20 mitochondria damaged (10.0%). These data are summarized in Table 2. To determine whether more damaged mitochondria are present in EAE axons than in control axons, total proportion (pooled data) of damaged mitochondria from each tissue type (EAE and control) were compared. Using a Fisher's exact test, the proportion of damaged mitochondria in EAE axons was significantly larger than the proportion of damaged mitochondria in control axons ($p < 0.001$).

Mitochondrial Shape Factor

Although we found a number of mitochondria with defects in both control and EAE animals, we noticed qualitative differences in both normal and damaged mitochondria between these two groups (Figure 5). In general, mitochondria in control axons retained their original shape whether they were damaged or not. That is, they remained slightly longer than they are wide (resembling a capsule) and remained parallel to the axis of the axon. Damaged and normal mitochondria in EAE axons appeared more sphere-like. To quantify this effect, we developed an index we call the "shape factor" where we divided mitochondrial length by the mitochondrial width for each mitochondrion examined in all EAE and control axons.

Mean shape factor for normal and damaged mitochondria were calculated for EAE axons (Table 3). The mean shape factor for normal mitochondria was 1.277 and 2.328 for EAE axons 1 and 2, respectively. The mean shape factor for

damaged mitochondria was 1.224 and 1.415 for EAE axons 1 and 2, respectively. Mean shape factor for normal and damaged mitochondria were calculated for control axons (Table 3). The mean shape factor for normal mitochondria from control axon 1 was 3.791, whereas the mean shape factor for damaged mitochondria was 1.734. The mean shape factor for normal mitochondria from control axon 2 was 2.535 compared to the damaged mitochondria mean shape factor of 2.794. All mitochondria from control axon 3 were classified normal with a mean shape factor of 5.769. Finally, the mean shape factor for normal mitochondria was 4.223 in control axon 4, and the mean shape factor for damaged mitochondria was 2.024.

To determine whether shape factor differed between mitochondria in EAE axons and control axons, mean shape factor for each category was compared by two-sample t-test. Mean shape factor for EAE mitochondria was significantly lower than mean shape factor for mitochondria in control axons ($p < 0.001$). This suggests that mitochondria in EAE axons tend to develop a spherical morphology that differs significantly from control axon mitochondria. Within each group, mean shape factor for damaged and control axons was also calculated. A two-sample t-test was used to determine that within each tissue type (EAE and control), damaged mitochondria exhibited a significantly lower shape factor than normal mitochondria (EAE $p < 0.001$, control $p = 0.019$). This suggests that damaged mitochondria tend to become spherical in shape.

During ultrastructural evaluation, we noticed that there were qualitative differences between even the damaged mitochondria in EAE tissue compared to the damaged mitochondria in control tissue. We wondered whether shape factor reflected those differences. We compared the mean shape factor of damaged EAE mitochondria and damaged control mitochondria using a two-sample t-test, and we found that EAE damaged mitochondria exhibit a significantly lower shape factor than control damaged mitochondria ($p < 0.001$). We also compared normal mitochondria from each group in the same way. Shape factor for normal mitochondria is significantly lower in EAE axons than in normal axons ($p < 0.001$). Within the control group, three axons expressed variants of GFP and one axon did not. To eliminate the possibility of GFP causing increased or decreased shape factor, we compared the mean shape factor by two-sample t-test from GFP mitochondria to those found in the non-GFP control axon. We found that the shape factor was largely similar between the two types of control axons ($p = 0.927$). Together, these results suggest that damage in control axons and EAE are morphologically distinct and may represent mechanistically separate cellular mechanisms.

Disruption of cytoskeletal arrangement

The previous results suggest mitochondria may be an early mediator of axon loss. Since we were able to view subcellular structures in their entirety, we were interested in knowing whether or not other ultrastructural characteristics

accompanied the mitochondrial pathology such as cytoskeletal abnormalities. Ordinarily the cytoskeleton maintains a linear, axial arrangement which is important for axonal transport. EAE and control axons identified by NIRB were examined for any inconsistencies with normal cytoskeletal arrangement. Concurrent with mitochondrial damage in EAE axons, disruption of cytoskeletal arrangement was revealed (Figure 6). Compared to cytoskeletal arrangement of control animals in which microtubules are arranged in a linear, regular pattern, neurofilaments in EAE axons appeared disorganized in places. In particular, neurofilaments often were arranged perpendicular to the long axis of the axon. Such an arrangement might compromise the cargo transported via these cytoskeletal elements. The cytoskeletal disruption we observed was not widespread throughout the axon, but rather seemed localized to areas populated by disrupted mitochondria.

Myelin removal

Because we targeted axons destined for degeneration, we were interested in additional factors contributing to an axon's degeneration including the relationship between immune cells and myelin. We were particularly focused on understanding the relationships at the interface between immune cells and myelin. By viewing direct and/or indirect contact between macrophages and myelin at various stages of demyelination, it is possible that we could determine certain qualities of the act of demyelination. In addition to the axons we targeted

for reconstruction, we viewed an additional ~50 axons per animal, many of which were in direct contact with an immune cell(s). We were surprised to notice that in many axons with obvious mitochondrial pathology, there was no immediate immune cell interaction. This observation suggests it is possible to have early events of axon pathology without direct local immune cell interaction. However, we noticed that it was common to detect compact portions of myelin entirely trapped within macrophages throughout the tissue. This observation raised two possibilities: 1.) Is myelin removed in bulk by mass disruption of multiple layers at once, or 2.) is myelin removed in a more subtle piecemeal method of disruption whereby small pieces of myelin are chipped away. It is also possible that myelin ends up within macrophages by a mechanism the reverse of its formation: that is, an unraveling in a single continuous sheet. However, this possibility seems less plausible due to the appearance of compact myelin trapped within immune cells. Regardless, each of these different mechanisms would have distinct structural and spatial features which would be revealed by electron microscopy, provided any of these mechanisms occurring during the time of tissue preservation and we were able to slice through these areas.

Out of over 100 axons observed through serial sections, we were able to pinpoint a particularly striking immune cell interaction that was likely the ultrastructural correlate of demyelination (Figure 7). On one axon, two multiple layered myelin segments that had delaminated from the main myelin sheath of the axon and were separated from the main axon but not completely

disconnected. The delaminated, separated myelin resembled an omega shape and was within the grasp (contained between immune cell processes) of two adjacent immune cells. The appearance of the omega shaped myelin layers connected by a very thin stalk of myelin contained within the immune cell suggests that multiple myelin layers can be removed simultaneously. Further, the immune cell appears to be actively engaged during demyelination as opposed to acting as a scavenger of dissociated myelin.

Discussion

Historically, neurodegenerative research has mostly focused upon proximate causes of disease with the idea of preventing the cascade of events at its inception. The motivation for this notion was that once a nerve cell or axon was compromised they all succumb through a conserved cellular pathway. Therefore, focusing upon preventing the earliest stages was strategically the best way to prevent disease. This idea is challenged by the idea that nerve cells do not necessarily degenerate through a conserved cellular mechanism. These results largely describe a novel mechanism where focal lesion sites induced by mitochondrial abnormalities induce axonopathy. The focal axonal swelling along with the relative mix of damaged and normal mitochondria is suggestive that a novel mechanism for axonal degeneration is taking place in EAE degeneration.

Known types of degeneration including Wallerian degeneration and axosome shedding are each associated with unique subcellular events. During Wallerian degeneration, axons degenerate *in toto* where mitochondria throughout an entire axon degenerate rapidly and the cytoplasm becomes electron lucent (B. Beirowski et al., 2005). Axosomal shedding is a form of axon loss during development where small pieces of axon that contain normal axonal constituents are shed to nearby glial cells (D. L. Bishop et al., 2004). In this way, axons are removed in a piecemeal fashion without creating a massive immune response as would be initiated during Wallerian degeneration. Focal swelling and localized mitochondrial pathology does not fit into any of the known categories of axon degeneration.

Near Infrared Burning (NIRB) – A novel approach to correlative light and electron microscopy.

Elucidating the events that underlie axon degeneration in the EAE model of MS required developing a new imaging technique. By taking advantage of high-power femtosecond-pulsed lasers, we were able to create fiducial markers that permitted routine correlated *in vivo* time lapse microscopy with serial section transmission electron microscopic reconstruction.

Currently, to study a disease progression over time at the cellular level, the method of choice is *in vivo* time-lapse imaging (T. Misgeld and M. Kerschensteiner, 2006). This imaging method can be useful in providing a chronology of major cellular events, but cannot resolve associated subcellular changes during disease. Viewing subcellular ultrastructure currently falls under the domain of electron microscopy. Until now, electron microscopic investigation provides a highly resolved view of a large sample that contains many items, many of which are not of interest. For example, in an EAE spinal cord TEM section containing ~1000 axons, axons will be in a continuum from healthy to degenerated. Therefore, each axon would have to be thoroughly examined for a predetermined characteristic that may prove to be unreliable. The results would be predicated upon chance that the correct characteristic was chosen and that an axon was actually imaged in the early stages of degeneration. Using a technique that relies on ambiguous correlation would not allow us to confidently place an axon temporally in the context of the disease process. Accurate

conclusions about the true disease process may or may not be reached based on the results of such a study.

One way to unite the temporal resolution provided by time-lapse *in vivo* imaging with the spatial resolution provided by EM is to correlate the techniques. Correlation of the techniques involves viewing the same axons at the light level over time and then examining the exact same axon at the EM level. The difficulty with this technique lies in finding an appropriate method to re-locate specific axons without obscuring subcellular structures. Since the electron microscope cannot see color in the traditional sense, differentiating cells amongst a population requires rendering selective tissues electron dense. Traditionally, this approach required using antibodies to a specific cell (i.e., anti-GFP to a GFP labeled cell) followed by secondary antibody conjugation to horseradish peroxidase to selectively label a cell (K. Herrmann et al., 1994; J. T. Trachtenberg et al., 2002). An alternate approach is to label a cell with a photoconvertible fluorophore and bleach the fluorophore in the presence of DAB (R. L. Calabrese and A. R. Maranto, 1986; J. Lubke, 1993). Both approaches are useful for relocating axons, but rely on increased electron density within an axon as the identifiable marker. Unfortunately, these methods often mask subcellular features and, in the case of antibodies, require permeabilizing tissue which severely degrades ultrastructure.

Our new approach of marking spinal cord tissue with a precisely controlled laser method we dubbed *near infrared burning* (NIRB) is the first technique that

allows individual axons in previously imaged tissue to be routinely re-identified at the EM level and examined without hindrance from a labeling procedure. In this project, implementing the NIRB technique in the early stages of degeneration (focally swollen, paranodal regions) in a MS mouse model allowed successful correlation between *in vivo* imaging of the degeneration process and ssTEM reconstruction. With this technique, we could unequivocally determine the subcellular ultrastructure of axons during early degeneration.

Mitochondrial pathology underlies unique mechanism of axon degeneration

Focally swollen, paranodal regions in EAE axons were identified during *in vivo* time lapse imaging, marked with NIRB, and targeted for ssTEM reconstruction. The ultrastructural evaluation of the axonal content revealed a unique mitochondrial pathology and an increased proportion of damaged mitochondria in EAE axons as compared to control axons. Damaged mitochondria in EAE axons appeared electron lucent and vesiculated, with disrupted cristae. This homogenous population of damaged and normal mitochondria suggests that one or more feature(s) of an EAE axon's internal environment, specifically within the swollen paranodal region, is associated with the mitochondrial pathology described.

One notable observation was that mitochondria can be damaged without the apparent loss of myelin. Further, some EAE axons with damaged

mitochondria had normal appearing myelin sheaths with no visible immune interaction. An alternative that we were unable to locate was axons with obvious myelin loss with normal appearing mitochondria. This lack of immune mediated demyelination at paranodal swellings is evidence that demyelination is likely not the proximate cause of axon degeneration.

Because we were unable to find disruption of both the myelin sheath and the axolemma, it is possible that degeneration is due to an intracellular mechanism rather than immune cell induced. Support for such an idea comes from a recent study by Ouardouz et al. that cites an internally activated Ca⁺ ionic imbalance as a possible trigger of axonal degeneration independent of demyelination (M. Ouardouz et al., 2009). Intracellular stores of Ca⁺ are released as a result of excess glutamate that initiates a cascade reaction beginning with the activation of a neurotransmitter receptor subunit, GluR6 in the presence of nitric oxide (NO) synthase. Downstream events to this excess calcium are not clear, but excitotoxic events associated with glutamatergic synapse activation are known to activate apoptotic pathways or caspases (M. Arundine and M. Tymianski, 2003). These caspases may be targeting mitochondria in such a scenario.

Cellular Mechanisms of Demyelination

Although our results suggest a separation of demyelination and axon degeneration during the EAE mouse model of MS, they cannot rule out the idea that ingested myelin by immune cells does not initiate signaling cascades that can injure axons. It is possible the way myelin is removed can influence the immune response and the axon. For instance, antigen load is well known to alter immune responses. Because multiple layers of myelin were being disrupted simultaneously, large pieces of myelin are being internalized by immune cells. Which pathways are activated through myelin ingestions are not entirely clear (T. Schmitz and L. J. Chew, 2008). Because sheets of myelin are simultaneously being disrupted, it is not unreasonable to infer that the entire myelin sheath integrity is compromised. But how far does this effect extend laterally? And how many layers are truly disrupted? Our results cannot completely answer these questions, but they can attest to the idea that diffusible proteases could be disrupting myelin proteins holding layers together.

Multiple sclerosis is a complex disease. Demyelination has long been the major focus of MS research, but axon damage seems to be emerging as the clear cause of steady CNS functional decline which occurs during the irreversible, progressive degeneration phase of the disease. However, the current thought is that axon damage begins during early stages independent of direct immune mediated demyelination, and accumulates throughout the progression of the disease including periods of recovery. Progressive decline

occurs when remyelination and other natural rehabilitation methods are finally helpless in compensating for axon loss.

The etiology of the disease is unknown, and therefore the exact causal relationship between the various aspects of the disease including demyelination, immune mediated inflammation, and axon damage is elusive. Specifically, do immune cell interactions directly instigate not only demyelination but also axon degeneration? Our results seem to suggest that while immune cell interaction is at the root of the disease, direct interaction with myelin is not necessary to cause axon degeneration. Perhaps this is why the current primary treatment for MS, immune suppression, has been successful in early stages of MS, but has thus not been effective in preventing irreversible CNS damage responsible for latter phases of the disease (G. C. Ebers et al., 2008). The results of this study present compelling evidence for a novel mechanism for axon degeneration characterized by focal axonal swelling and mitochondrial pathology.

References

- Arundine M, Tymianski M (2003) Molecular mechanisms of calcium-dependent neurodegeneration in excitotoxicity. *Cell Calcium* 34:325-337.
- Beirowski B, Adalbert R, Wagner D, Grumme DS, Addicks K, Ribchester RR, Coleman MP (2005) The progressive nature of Wallerian degeneration in wild-type and slow Wallerian degeneration (Wlds) nerves. *BMC Neurosci* 6:6.
- Bishop DL, Misgeld T, Walsh MK, Gan WB, Lichtman JW (2004) Axon branch removal at developing synapses by axosome shedding. *Neuron* 44:651-661.
- Bjartmar C, Trapp BD (2001) Axonal and neuronal degeneration in multiple sclerosis: mechanisms and functional consequences. *Curr Opin Neurol* 14:271-278.
- Bjartmar C, Wujek JR, Trapp BD (2003) Axonal loss in the pathology of MS: consequences for understanding the progressive phase of the disease. *J Neurol Sci* 206:165-171.
- Bueler H (2009) Impaired mitochondrial dynamics and function in the pathogenesis of Parkinson's disease. *Exp Neurol*.
- Calabrese RL, Maranto AR (1986) Cholinergic action on the heart of the leech, *Hirudo medicinalis*. *J Exp Biol* 125:205-224.
- Culmsee C, Landshamer S (2006) Molecular insights into mechanisms of the cell death program: role in the progression of neurodegenerative disorders. *Curr Alzheimer Res* 3:269-283.
- de la Cruz RR, Pastor AM, Delgado-Garcia JM (1996) Influence of the postsynaptic target on the functional properties of neurons in the adult mammalian central nervous system. *Rev Neurosci* 7:115-149.
- Dutta R, Trapp BD (2007) Pathogenesis of axonal and neuronal damage in multiple sclerosis. *Neurology* 68:S22-31; discussion S43-54.
- Ebers GC, Heigenhauser L, Daumer M, Lederer C, Noseworthy JH (2008) Disability as an outcome in MS clinical trials. *Neurology* 71:624-631.
- Feng G, Mellor RH, Bernstein M, Keller-Peck C, Nguyen QT, Wallace M, Nerbonne JM, Lichtman JW, Sanes JR (2000) Imaging neuronal subsets in transgenic mice expressing multiple spectral variants of GFP. *Neuron* 28:41-51.
- Fiala JC, Harris KM (2001) Cylindrical diameters method for calibrating section thickness in serial electron microscopy. *J Microsc* 202:468-472.
- Hauser SL, Oksenberg JR (2006) The neurobiology of multiple sclerosis: genes, inflammation, and neurodegeneration. *Neuron* 52:61-76.
- Herrmann K, Antonini A, Shatz CJ (1994) Ultrastructural evidence for synaptic interactions between thalamocortical axons and subplate neurons. *Eur J Neurosci* 6:1729-1742.
- Kalman B, Laitinen K, Komoly S (2007) The involvement of mitochondria in the pathogenesis of multiple sclerosis. *J Neuroimmunol* 188:1-12.
- Kerschensteiner M, Stadelmann C, Buddeberg BS, Merkler D, Bareyre FM, Anthony DC, Linington C, Bruck W, Schwab ME (2004) Targeting experimental autoimmune encephalomyelitis lesions to a predetermined axonal tract system allows for refined behavioral testing in an animal model of multiple sclerosis. *Am J Pathol* 164:1455-1469.
- Knott AB, Perkins G, Schwarzenbacher R, Bossy-Wetzel E (2008) Mitochondrial fragmentation in neurodegeneration. *Nat Rev Neurosci* 9:505-518.
- Kornek B, Storch MK, Weissert R, Wallstroem E, Stefferl A, Olsson T, Linington C, Schmidbauer M, Lassmann H (2000) Multiple sclerosis and chronic autoimmune encephalomyelitis: a

- comparative quantitative study of axonal injury in active, inactive, and remyelinated lesions. *Am J Pathol* 157:267-276.
- Lubke J (1993) Photoconversion of diaminobenzidine with different fluorescent neuronal markers into a light and electron microscopic dense reaction product. *Microsc Res Tech* 24:2-14.
- Misgeld T, Kerschensteiner M (2006) In vivo imaging of the diseased nervous system. *Nat Rev Neurosci* 7:449-463.
- Misgeld T, Nikic I, Kerschensteiner M (2007) In vivo imaging of single axons in the mouse spinal cord. *Nat Protoc* 2:263-268.
- Mutsaers SE, Carroll WM (1998) Focal accumulation of intra-axonal mitochondria in demyelination of the cat optic nerve. *Acta Neuropathol* 96:139-143.
- Ouardouz M, Coderre E, Basak A, Chen A, Zamponi GW, Hameed S, Rehak R, Yin X, Trapp BD, Stys PK (2009) Glutamate receptors on myelinated spinal cord axons: I. GluR6 kainate receptors. *Ann Neurol* 65:151-159.
- Papadopoulos D, Pham-Dinh D, Reynolds R (2006) Axon loss is responsible for chronic neurological deficit following inflammatory demyelination in the rat. *Exp Neurol* 197:373-385.
- Qi X, Lewin AS, Sun L, Hauswirth WW, Guy J (2006) Mitochondrial protein nitration primes neurodegeneration in experimental autoimmune encephalomyelitis. *J Biol Chem* 281:31950-31962.
- Rivers TM (1935) Encephalomyelitis accompanied by myelin destruction experimentally produced in monkeys. *J Exp Med* 61:689-702.
- Schmitz T, Chew LJ (2008) Cytokines and myelination in the central nervous system. *ScientificWorldJournal* 8:1119-1147.
- Sherman DL, Brophy PJ (2005) Mechanisms of axon ensheathment and myelin growth. *Nat Rev Neurosci* 6:683-690.
- Skundric DS (2005) Experimental models of relapsing-remitting multiple sclerosis: current concepts and perspective. *Curr Neurovasc Res* 2:349-362.
- Thress K, Kornbluth S, Smith JJ (1999) Mitochondria at the crossroad of apoptotic cell death. *J Bioenerg Biomembr* 31:321-326.
- Trachtenberg JT, Chen BE, Knott GW, Feng G, Sanes JR, Welker E, Svoboda K (2002) Long-term in vivo imaging of experience-dependent synaptic plasticity in adult cortex. *Nature* 420:788-794.
- Trapp BD, Ransohoff R, Rudick R (1999) Axonal pathology in multiple sclerosis: relationship to neurologic disability. *Curr Opin Neurol* 12:295-302.
- Vila M, Perier C (2008) Molecular pathways of programmed cell death in experimental Parkinson's disease. *Parkinsonism Relat Disord* 14 Suppl 2:S176-179.
- Wang X, Zhu S, Pei Z, Drozda M, Stavrovskaya IG, Del Signore SJ, Cormier K, Shimony EM, Wang H, Ferrante RJ, Kristal BS, Friedlander RM (2008) Inhibitors of cytochrome c release with therapeutic potential for Huntington's disease. *J Neurosci* 28:9473-9485.
- Williamson TL, Cleveland DW (1999) Slowing of axonal transport is a very early event in the toxicity of ALS-linked SOD1 mutants to motor neurons. *Nat Neurosci* 2:50-56.

Tables

Table 1

Axon	Total Mitochondria Quantified	Normal	Damaged	Proportion damaged
EAE Axon 1	107	76	31	0.290
EAE Axon 2	32	14	18	0.562
Total	139	90	49	0.353

Table 1. Axons from experimental autoimmune encephalomyelitis (EAE) axons contained a higher proportion of damaged mitochondria than control axons. All mitochondria from two EAE axons were qualitatively examined for structural damage. Mitochondria which appeared electron bare, vesiculated, and lacked organized cristae were considered damaged. Mitochondria were considered normal if only one or two of these characteristics was visible. The total proportion of bad mitochondria in EAE axons was 35.3%. This proportion was significantly higher than the proportion of damaged mitochondria in control axons (see table 2, $p < 0.001$).

Table 2

Axon	Total quantified	Normal	Damaged	Proportion damaged
GFP Control 1 (not imaged)	33	30	3	0.091
GFP Control 2 (not imaged)	60	47	13	0.217
GFP Control 3 (imaged)	61	61	0	0.000
non-GFP Control 4 (not imaged)	20	18	2	0.100
Total	174	157	18	0.103

Table 2. Mitochondria from control axons contained a smaller proportion of damaged mitochondria than experimental autoimmune encephalomyelitis (EAE) axons. Mitochondria from four axons were qualitatively examined for structural damage. Mitochondria were considered normal if only one or two structural characteristics was compromised (electron density, cristae organization, or vesiculation). Mitochondria were considered damaged in all three structural characteristics were compromised. The total proportion of damaged mitochondria was 10.3%. This proportion was significantly less than the proportion of damaged mitochondria in EAE axons (see table 1, $p < 0.001$).

Table 3

	Mean Shape Factor: Normal	Mean Shape Factor: Damaged
EAE Axon 1	1.277	1.224
EAE Axon 2	2.328	1.415
GFP Control 8a (not imaged)	3.791	1.734
GFP Control 8b (not imaged)	2.535	2.794
GFP Control 8c (imaged)	5.769	-
Non-GFP Control 8d (not imaged)	4.223	2.024

Table 3. Mitochondrial shape factor was significantly lower for normal mitochondria within each group (EAE and control); shape factor for normal and damaged mitochondria was lower for EAE axons as compared to their control axon counterpart groups. The mean shape factor for normal mitochondria was significantly higher than the mean shape factor for damaged mitochondria in both control and EAE axons (control $p = 0.019$, EAE $p < 0.001$). The mean shape factor also differed between control axons and EAE axons within mitochondrial classifications. The mean shape factor for normal mitochondria was significantly higher in control axons compared to EAE axons ($p < 0.001$). The mean shape factor for damaged mitochondria was also significantly higher for mitochondria from control axons compared to those from EAE axons ($p < 0.001$).

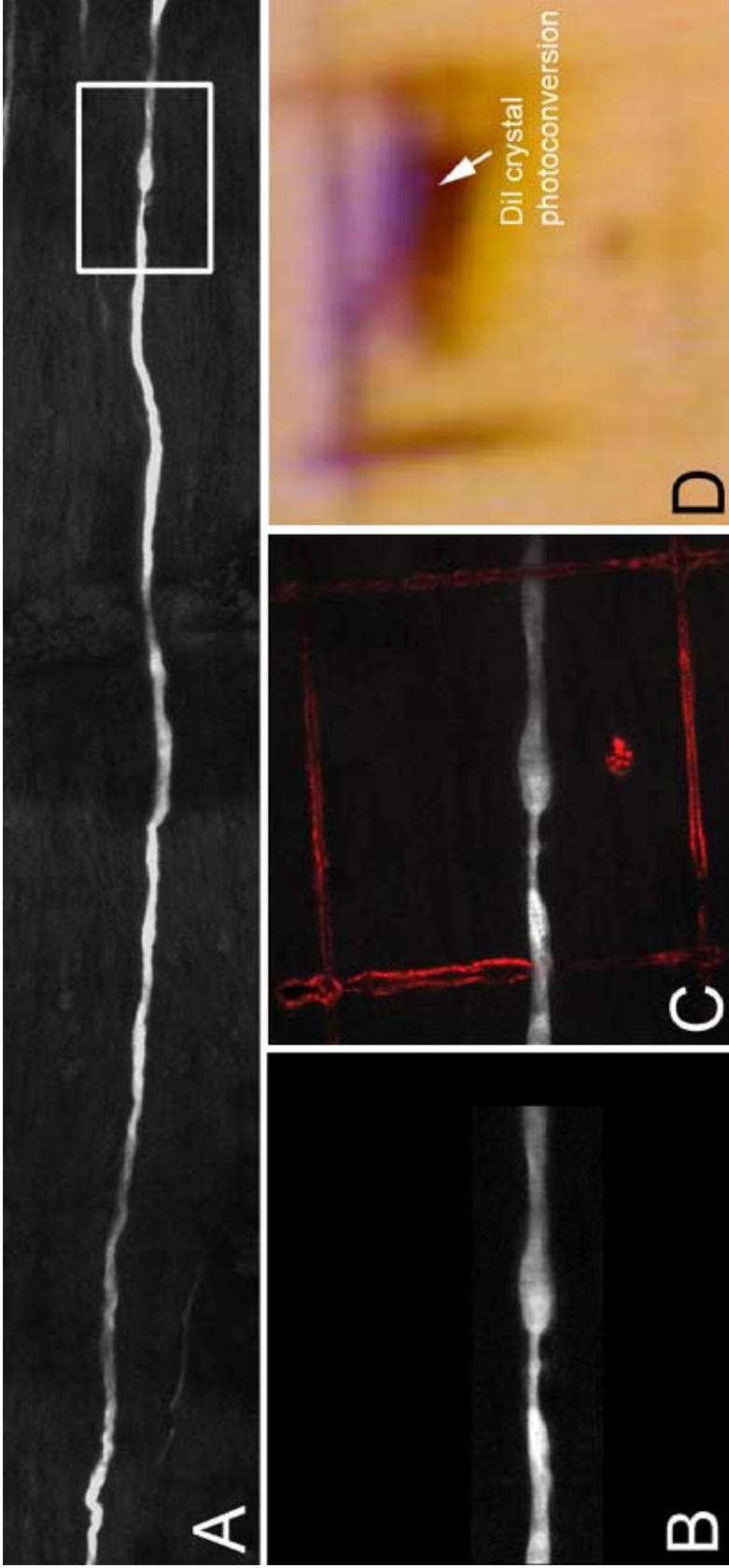


Figure 1. Laser-induced Fiducial Markers. **A.** A low magnification confocal reconstruction of an entire spinal cord axon from an experimental autoimmune encephalomyelitis (EAE) animal is shown *in vivo*. Boxed area containing a focal paranodal swelling is enlarged in panel **B**. **B.** A confocal reconstruction of the boxed region of interest in panel **A** is enlarged. **C.** The same region of interest is shown within a box (red) created by a mode-locked Ti:sapphire laser. A small fiducial marker (arrow) has been burned adjacent to axon of interest. **D.** A crystal of 1,1'-dioctadecyl-3,3',3'-tetramethylindodicarbocyanine-5,5'-disulfonic acid (DiI) rendered electron dense following excitation in the presence of diaminobenzidine (DAB) was inserted in the tissue to serve as an additional fiducial marker (arrow). Also, autofluorescence from the laser burned box was rendered electron dense.

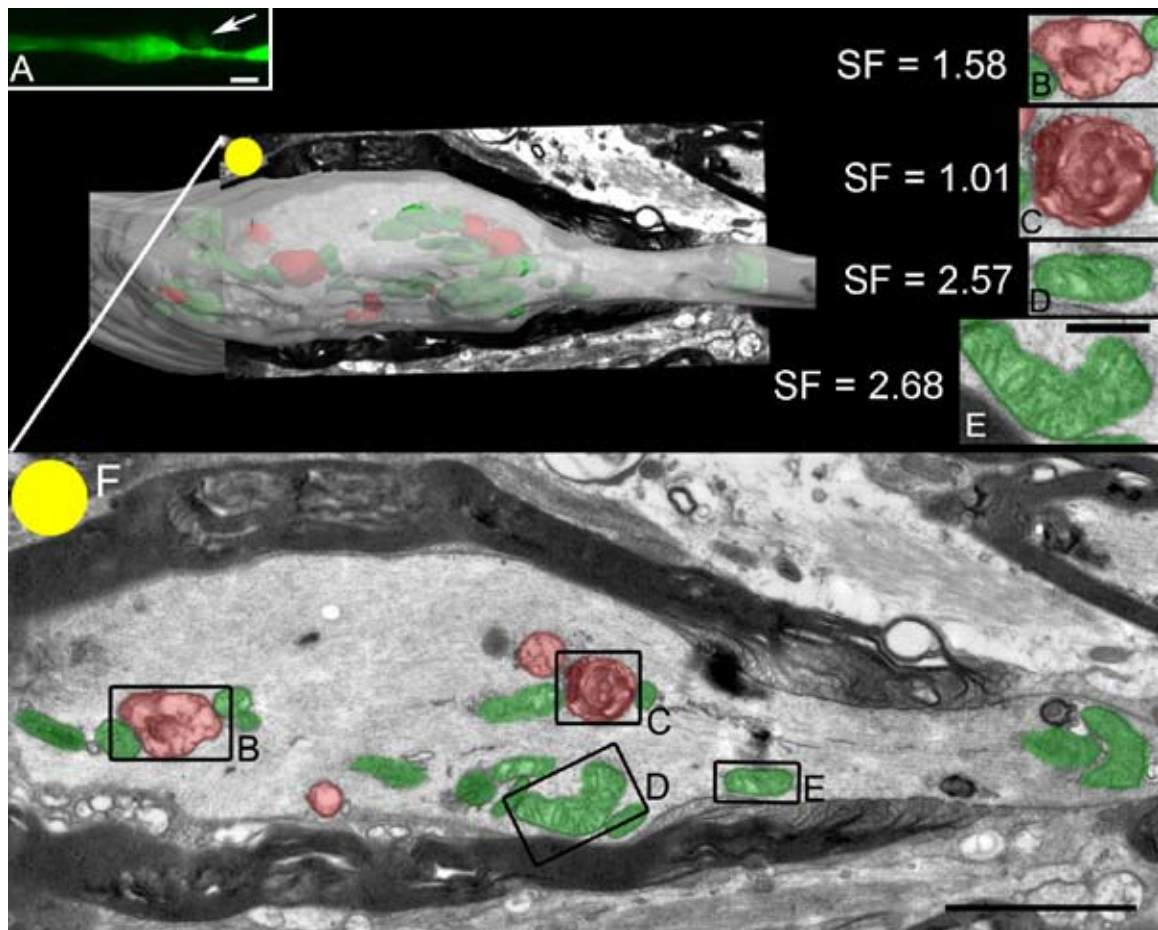


Figure 2. Correlated light and electron microscopy show early mitochondrial morphological changes in experimental autoimmune encephalomyelitis (EAE) axons. **A.** A confocal reconstruction of the paranodal region of an EAE axon shows morphology prior to degeneration. Arrow is pointing to an outpocketing of GFP from the axon. Scale bar = 3 microns. **B,C.** Damaged mitochondria were characterized by lack of organized cristae, vesiculation, and scarce electron density. Damaged mitochondria also had shape factor (SF) close to one. Damaged mitochondrion B had SF of 1.58, and damaged mitochondrion C had SF of 1.01. Scale bar for all mitochondria shown on panel E; scale bar = 0.5 micron. **D,E.** Normal mitochondria did not exhibit any vesiculation, contained organized cristae, and appeared electron dense. A mitochondrion was also considered normal if up to two of these characters were compromised. Normal mitochondria had SF larger than one and appeared elongated as opposed to rounded. Normal mitochondrion D had a SF of 2.57, and normal mitochondrion E had a SF of 2.68. Scale bar = 0.5 micron. **F.** An electron micrograph inserted into a surface rendering of the EAE axon and all mitochondria. Distribution of damaged and normal mitochondria are shown; damaged mitochondria are colored red and normal mitochondria are colored green.

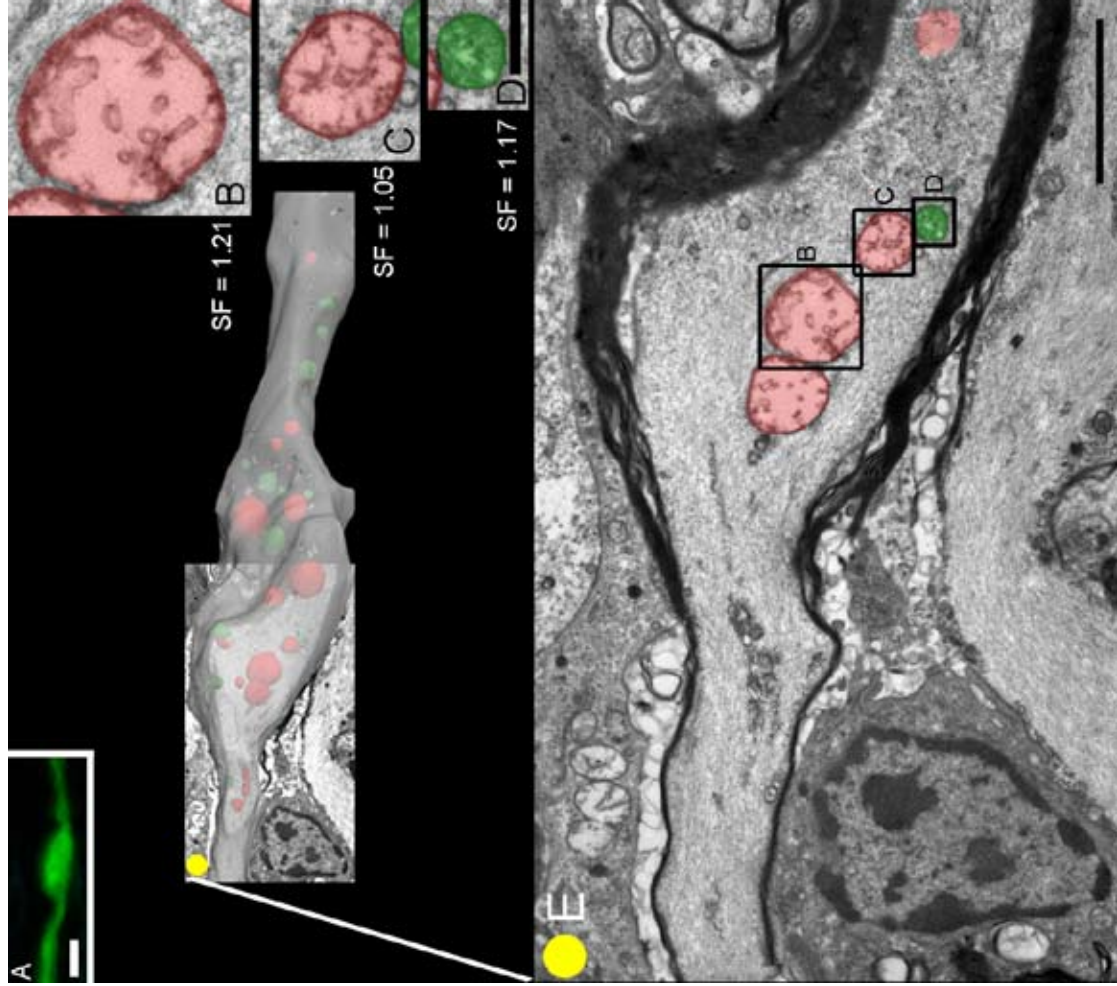


Figure 3. Correlated light and electron microscopy show early mitochondrial morphological changes in experimental autoimmune encephalomyelitis (EAE) axons. **A.** A confocal reconstruction of the paranodal region of an EAE axon shows morphology prior to degeneration. Scale bar = 4 microns. **B,C.** Damaged mitochondria were characterized by lack of organized cristae, vesiculation, and scarce electron density. Damaged mitochondria also had shape factor (SF) close to one. Damaged mitochondrion B had a SF of 1.21, and damaged mitochondrion C had a SF of 1.05. Scale bar for all mitochondria shown on D; scale bar = 0.5 micron. **D.** Normal mitochondria did not exhibit any vesiculation, contained organized cristae, and appeared electron dense. A mitochondrion was also considered normal if up to two of these characters were compromised. Normal mitochondria had SF larger than one and appeared elongated as opposed to rounded. Normal mitochondrion D had SF of 1.17. Scale bar = 0.5 micron. **F.** An electron micrograph inserted into a surface rendering of the EAE axon and all mitochondria. Distribution of damaged and normal mitochondria are shown; damaged mitochondria are colored red and normal mitochondria are colored green. Scale bar = 2 microns.

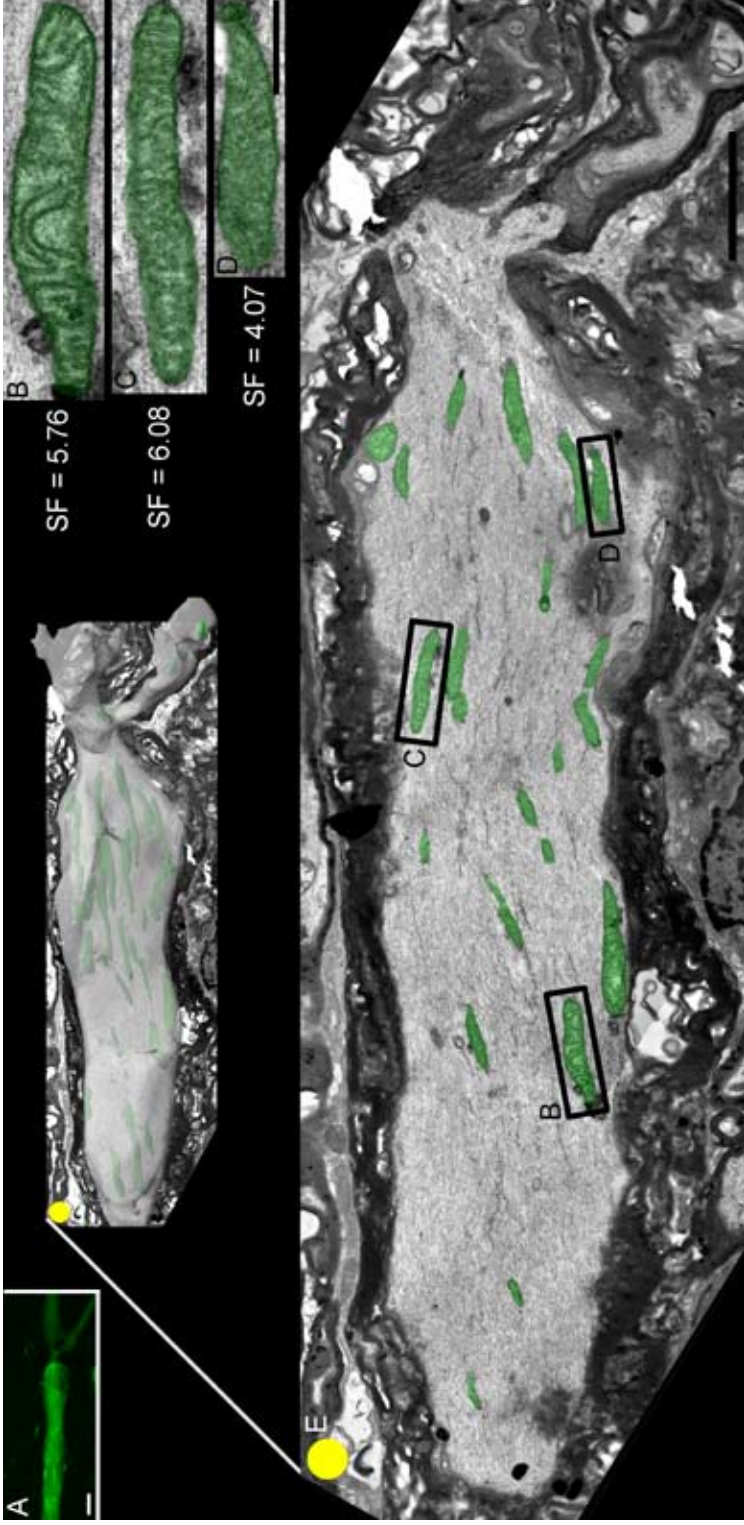


Figure 4. Correlated light and electron microscopy show normal mitochondrial morphology in a representative axon from control animals. **A.** A confocal reconstruction of the paranodal region of an EAE axon shows morphology prior to degeneration. Scale bar = 5 microns. **B,C,D.** Normal mitochondria did not exhibit any vesiculation, contained organized cristae, and appeared electron dense. A mitochondrion was also considered normal if up to two of these characters were compromised. Normal mitochondrion B had a SF of 5.67, SF for than one and appeared elongated as opposed to rounded. Normal mitochondrion C was 4.07, SF for 6.08, and SF for mitochondrion D was 4.07. Scale bar = 0.5 micron for panels B, C, D. **E.** An electron micrograph inserted into a surface rendering of the EAE axon and all mitochondria. Distribution of damaged and normal mitochondria are shown; no damaged mitochondria are shown in this section and normal mitochondria are colored green. Scale bar = 2.5 microns

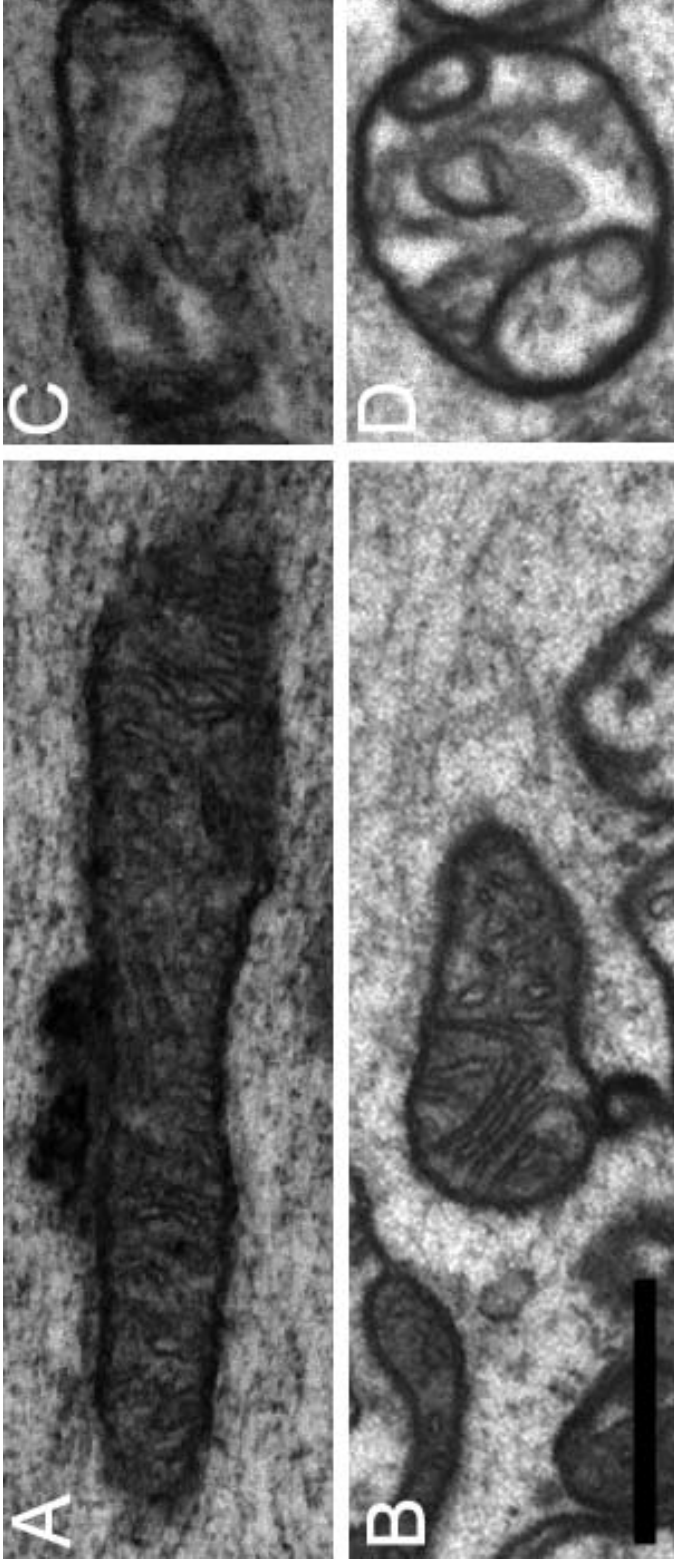


Figure 5. Shape factor of normal and damaged mitochondria is lower in EAE axons as compared to their control axon counterpart groups. Normal mitochondria in EAE axons, while meeting all normal criteria as described for this project, displayed a significantly lower mean shape factor than normal mitochondria in control axons ($p < 0.001$). Damaged mitochondria in EAE and control axons both met the same criteria, but damaged mitochondria in EAE axons had a significantly lower shape factor than damaged mitochondria in control axons ($p < 0.001$). **A.** A representative normal mitochondrion from control tissue appeared electron dense, had clearly organized internal cristae, and did not appear vesiculated; shape factor = 5.69. **B.** Normal mitochondrion from EAE axon met all normal criteria, but has a significantly lower shape factor = 2.03. **C.** Damaged mitochondrion from control tissue did not have any in tact cristae within the structure and also appeared electron dense and vesiculated. The mitochondrion remained slightly elongated, shape factor = 3.43. **D.** Damaged mitochondrion displays all damaged criteria and has almost equal length and width, shape factor = 1.606 . Scale bar 0.5 micron for all panels.

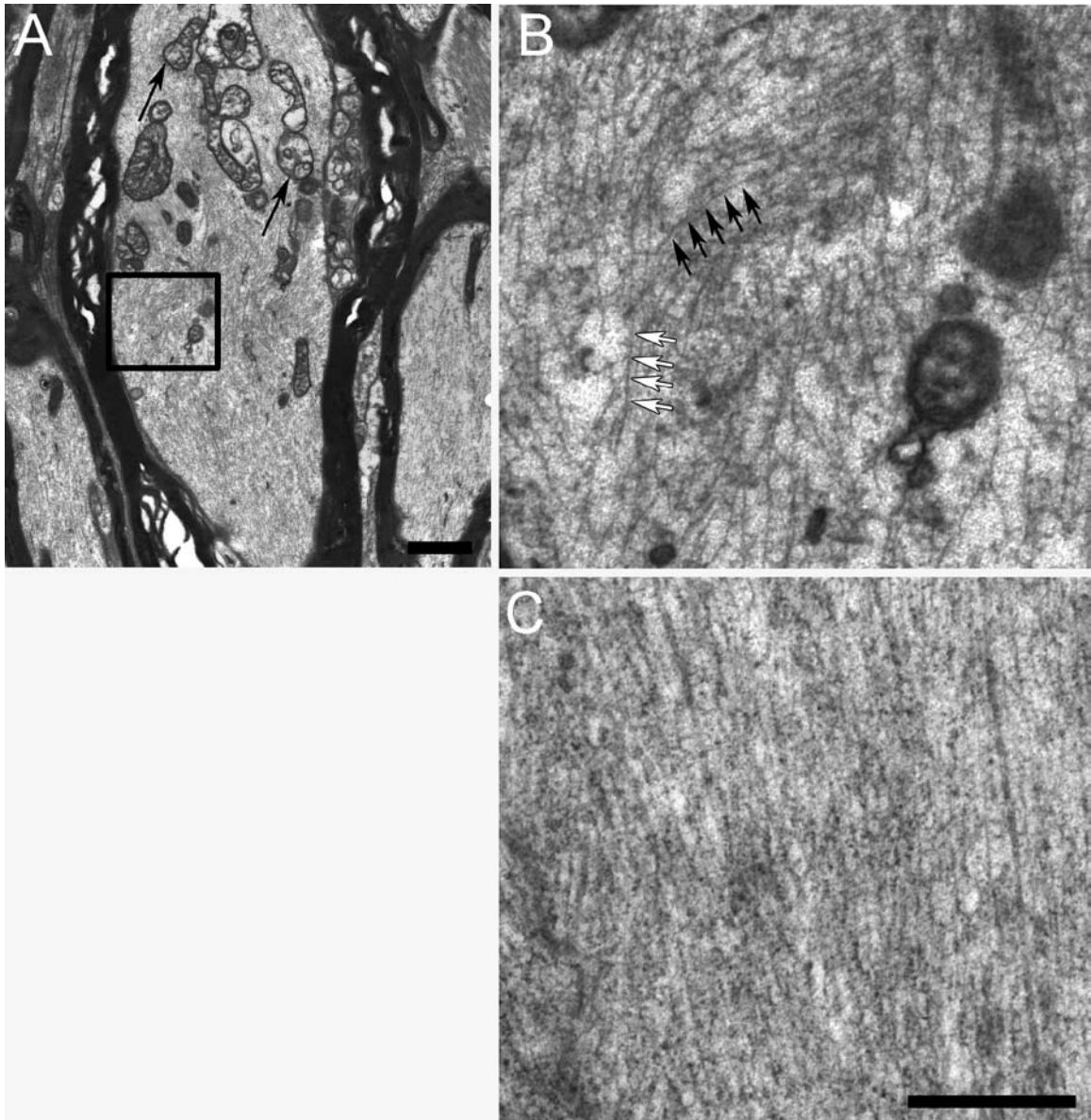


Figure 6. Disrupted cytoskeleton in EAE axons. **A.** A low magnification electron micrograph of EAE axon showing multiple damaged and normal mitochondria (arrows) also reveals non-linear cytoskeletal arrangement. The boxed region appears in panel B. Scale bar = 1.0 micron. **B.** Enlarged view of the boxed area of panel A gives a higher resolution view of neurofilaments which are not arranged parallel to each other and axial to the axon. Instead, microtubules are curvilinear. See arrows. Density of neurofilaments is reduced compared to control. Reference scale bar for panel C. **C.** Cytoskeleton of control axons appears linearly, axially arranged. Scale bar = 0.5 micron.

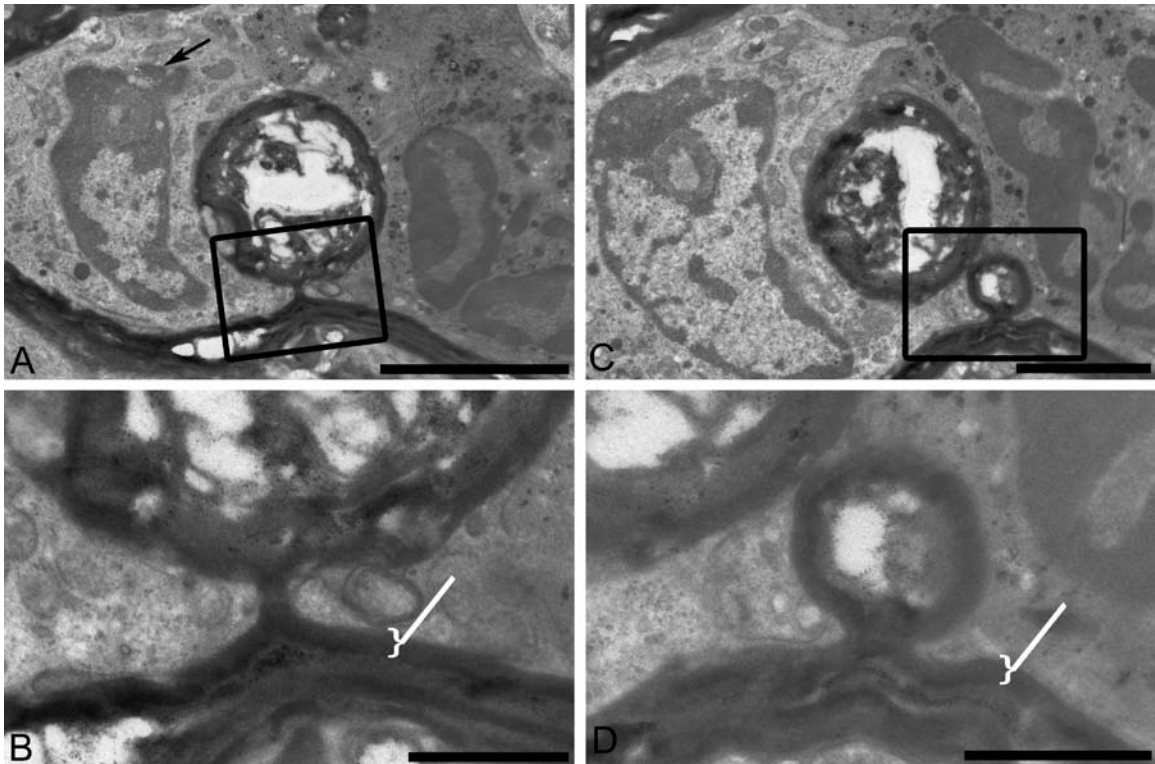


Figure 7. Demyelination through delamination of multiple myelin layers. **A.** A low magnification electron micrograph shows multiple layers of myelin largely dissociated from the main myelin sheath but connected by a thin stalk of myelin. Two immune cell nuclei are located on either side of the delaminated myelin (arrows). The boxed area is enlarged in panel B. Scale bar = 2.0 microns. **B.** A high magnification electron micrograph shows multiple myelin layers delaminated from the myelin sheath, but connected by a thin myelin stalk. Bracket marker defines the boundaries of a single layer of myelin. Scale bar = 0.5 micron. **C.** In the same axon, a few sections distal to the dissociated myelin structure in panels A,B, a second dissociated myelin structure is present. The boxed area is enlarged in panel D. Scale bar = 1.0 micron. **D.** Multiple layers of myelin are delaminated from the myelin sheath but remain connected by a thin myelin stalk. The bracket marker defines a single layer of myelin. Scale bar = 0.5 micron.